Supplementary Information

Virus particle assembly into crystalline domains enabled by the coffee ring effect

Ronald Gebhardt, Jean-Marie Teulon, Jean-Luc Pellequer, Manfred Burghammer, Jacques-Philippe Colletier and Christian Riekel

Substrate preparation. Glass cover slides were cleaned by means of a 5 min treatment with dichloromethane in an ultrasonic bath and rinsed with water afterwards. Organic traces were removed from the surface using an oxidation bath (1400 mL *Millipore* water, 120 mL H_2O_2, and 120 mL NH_3).[1] The glass cover slides were then stored in *Millipore* water until the beginning of the experiment.

TMV solution deposition. The solution was centrifuged and filtered. 2-µL droplets of ~3 nM TMV solution were deposited by a micropipette on a smooth glass slide at room temperature and cast after 10 min.

Dynamic Light Scattering. The field correlation function $g_1(\tau)$ was transformed into the intensity correlation function $g_2(\tau)$ via the Siegert relation.[2] Applying an implemented inverse Laplace transformation and the Stoke Einstein relation leads to a bimodal size distributions with peak maxima at D_1 = 75 nm and D_2 = 253 nm, which can be attributed to two diffusive modes along and perpendicular to the TMV fiber axis. (Fig. S1)

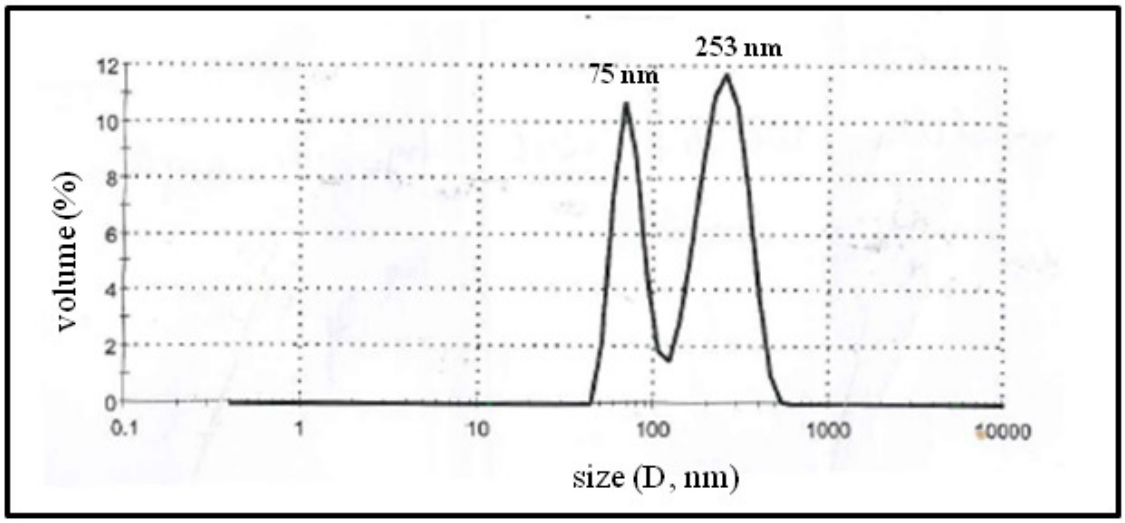

Fig. S1 Dynamic light scattering data for TMV solution

Deviations from the real values D_1 = 400 Å and D_2 = 3000 Å are due to the averaging over all orientations of the molecule in solution and to the fact that light scattering is biased towards larger-sized molecules.

Atomic Force Microscopy. We imaged the same sample used for X-ray diffraction experiments by a *Small Infinity* atomic force microscope (AFM) in tapping mode using a resonance frequency of 30 kHz and amplitude of 381 µV. Visualization was enabled by a FC2000 camera module (*Faymax*) equipped with a MLH-10X objective (*Computar*). The pixel resolution corresponded to about 100 Å. We fitted a Gaussian function to the scan-points of the line in Fig. 2 in order to determine the diameter of a TMV-rod.

Complimentary AFM experiments were performed for TMV particles which were purified from infected tobacco leaves of *Nicotiana tabacum var. Samsun* using several differential centrifugations.[3] Purified viruses (4.41 µM) were conserved in EDTA 1 mM, pH 7.7, at 4°C. The TMV solution was diluted 1/100 in water and 2 µl was deposited on round cover glass ∅ 8 mm (Decklaser). The drop was dried 3 hours at room temperature and imaged without additional treatment. AFM images of TMV crystals were recorded using the contact mode in air using a commercial Dimension D3100 (Bruker AXS, Santa Barbara) with a silicon probe (ESP, k = 0.2 N/m; nominal tip radius 8 nm; Bruker AFM probes) at a scan rate of 1 Hz. Compact TMV images were recorded using the Peak Force tapping mode (Bruker AXS) with a sharp nitride lever (SNL, k = 0.32 N/m, nominal tip radius 2 nm, Bruker AFM probes) at a scan rate of 0.7 Hz. Scan sizes for all images were 512 x 512 pixels. The raw AFM image shown in Fig. 2 was flattened using a polynomial function of 4th order in Gwyddion.[4]

Synchrotron radiation diffraction experiments. The pink beam from an ESRF undulator was monochromated to a wavelength of λ=0.997 Å and focused to ~1*1 µm^2 at the sample position.[5] Diffraction experiments were performed at room temperature in transmission- and reflection-geometry without sample rotation. (Fig. S2) The incidence angle in reflection-geometry of α_i=0.68^0 corresponds to grazing incidence small-angle X-ray scattering (GISAXS) conditions,[6, 7] translating to a beam footprint of ~84 µm on the substrate [6] and to an average X-ray penetration depth of ~2.5 µm. The beam footprint was aligned normal to the radial direction of the drop. The glass slide with the dried sample was placed on a two-axis goniometer (angles: α,ψ), mounted on a motorized x/y/z translation unit. Diffraction patterns in were collected with a MAR165 CCD at distance from of 772.3 (±0.5) mm from the sample with a typical exposure time per pattern of 20 sec. A silver behenate standard was used for distance calibration and to determine the instrumental resolution function.[8] X-ray diffraction patterns in transmission-geometry (Fig. S2) were collected using a FRELON camera[9] (2Kx2K pixels, 16-bit readout with 4x4 binning) at a distance of 136.3 (±0.2) mm from the sample. Distance calibration and determination of the instrumental resolution were performed using an α-Al_2O_3 powder standard (NBS: SRM 674a).[10] Positions on the sample were chosen using an on-axis optical Olympus microscope aligned with the focal spot of the micro-beam. In order to avoid radiation damage, exposure time was limited to 5 sec per pattern.

The patterns were examined and analyzed using the FIT2D software.[11] Integrated intensities (I_o) and sigma (σ_o) values were determined by summing the peak profiles in radial direction and fitting Gaussian functions to the azimuthal profiles. Structure factor amplitudes -F_o- were approximated to correspond to $\sqrt{I_o}$ and $\sigma_{F_{obs}} = 0.5 * \sqrt{\sigma_{I_o}}$. TMV structural parameters based on X-ray fiber diffraction [12] and cryo-TEM [13] were obtained from the RCSB Protein Data Bank (PDB IDs: 2TMV, 2OM3).

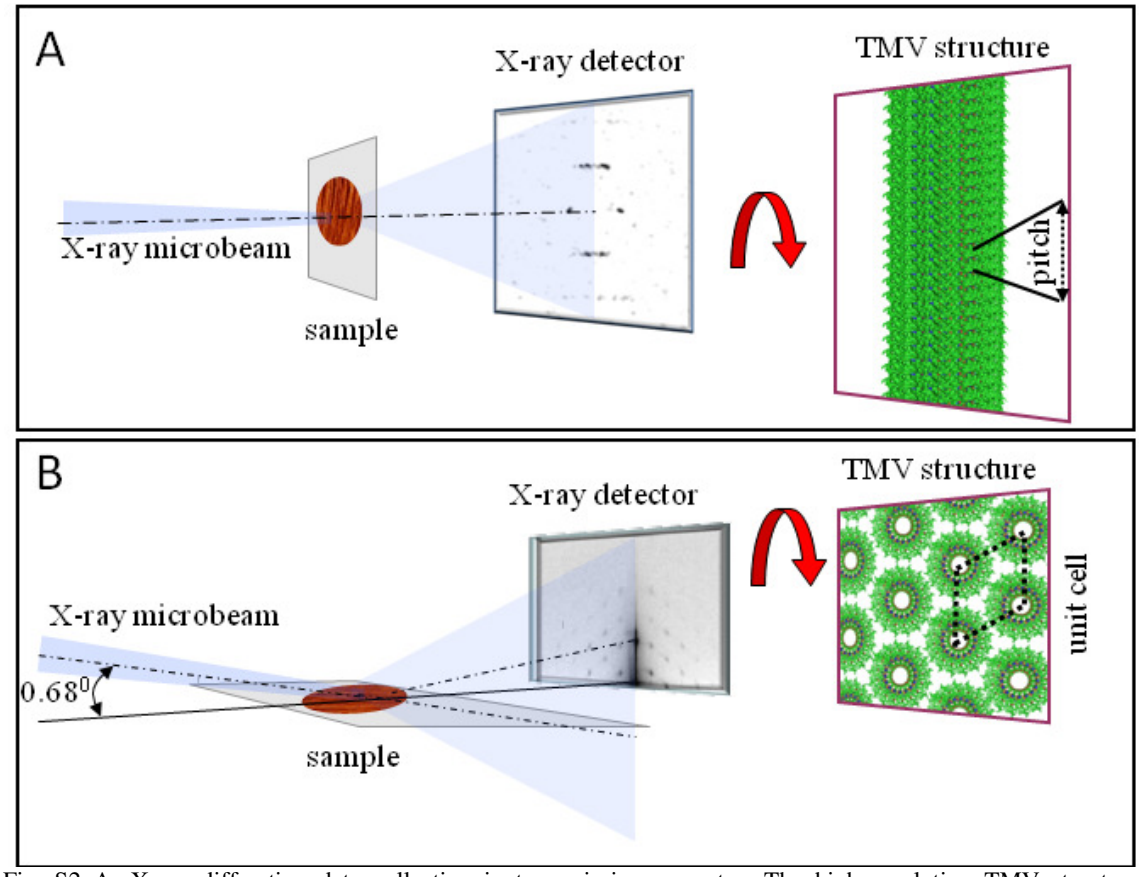

Fig. S2 A: X-ray diffraction data collection in transmission-geometry. The high resolution TMV structure determined by X-ray fiber diffraction is shown on the right panel.[12] B: X-ray diffraction data collection in low incidence angle reflection-geometry. The high resolution TMV structure determined by X-ray fiber diffraction is shown on the right panel.[12]

Calculation of electron density maps. The biological unit was generated using PDBSET from the CCP4 software suite,[14] after placing the starting monomer at the origin of a primitive triclinic cell (a=b=172 Å; c=69 Å; $\alpha=\beta=90$; $\gamma=120$). Calculated structure-factors (amplitudes and phases: F_c, ϕ_c) were generated using SFALL from the CCP4 software suite. Owing to the limited completeness and resolution of the observed data (I_o,F_o), no refinement was performed. Rather, we selected the subset of F_c and ϕ_c of reflections for which we had measured experimental intensities (SFTOOLS from the CCP4 software suite). Electron density maps were calculated, from either F_o and ϕ_c values or F_c and ϕ_c values. We also calculated difference electron density and composite maps based on either (F_o-F_c) or ($2F_o$-F_c) amplitudes and ϕ_c values. The maps were produced using PYMOL.[15]

X-ray beam penetration depth. Calculations[16] were based on the TMV composition[12] of $C_{793}N_{226}O_{331}P_3S$. The refraction index is calculated as n=0.9999938 according using the web page: henke.lbl.gov/optical_constants/getdb2.html. The average penetration depth (δ_p) is derived from $\delta_p = \frac{\sin \alpha_r}{\rho\mu}$. The angle of the reflected beam (α_r) is calculated from: $\sin\alpha_r=\mathrm{Re}[(n^2-\cos^2\alpha)^{0.5}]$ with Re the real part of a complex number. Based on the angle of the incoming beam of α= 0.68° one obtains α_r=0.63°. The mass absorption coefficient (μ/ρ) is

derived from the NIST data base (www.nist.gov/pml/data/xraycoef/) as μ/ρ=3291 cm^2/g. We used the density of myoglobin ρ=1.2 g/cm^3 providing an absorption coefficient of μ=3949 cm.[1] From the attenuation law $I / I_0 = e^{-1} = e^{\mu\delta_p}$ one obtains a path length δ_p =2.5 µm. We estimate that the thickness of the TMV boundary-rim is < 10 µm, i.e. in the same range as for a fibroin solution droplet.[6]

Raster transmission-diffraction. Raster-diffraction with 4 µm steps reveals the presence of domains (I,II) with homogeneous c-axis orientation at the outer edge of the boundary zone. (Fig. 2,S3) The presence of domains at the rim is also suggested by optical microscopy (Fig. S3). The structural homogeneity of domain I was explored based on the central part of the n=3 layer-line. (Fig. S4) The corresponding composite diffraction image suggests intensity variations of discrete reflections. (Fig. S4)

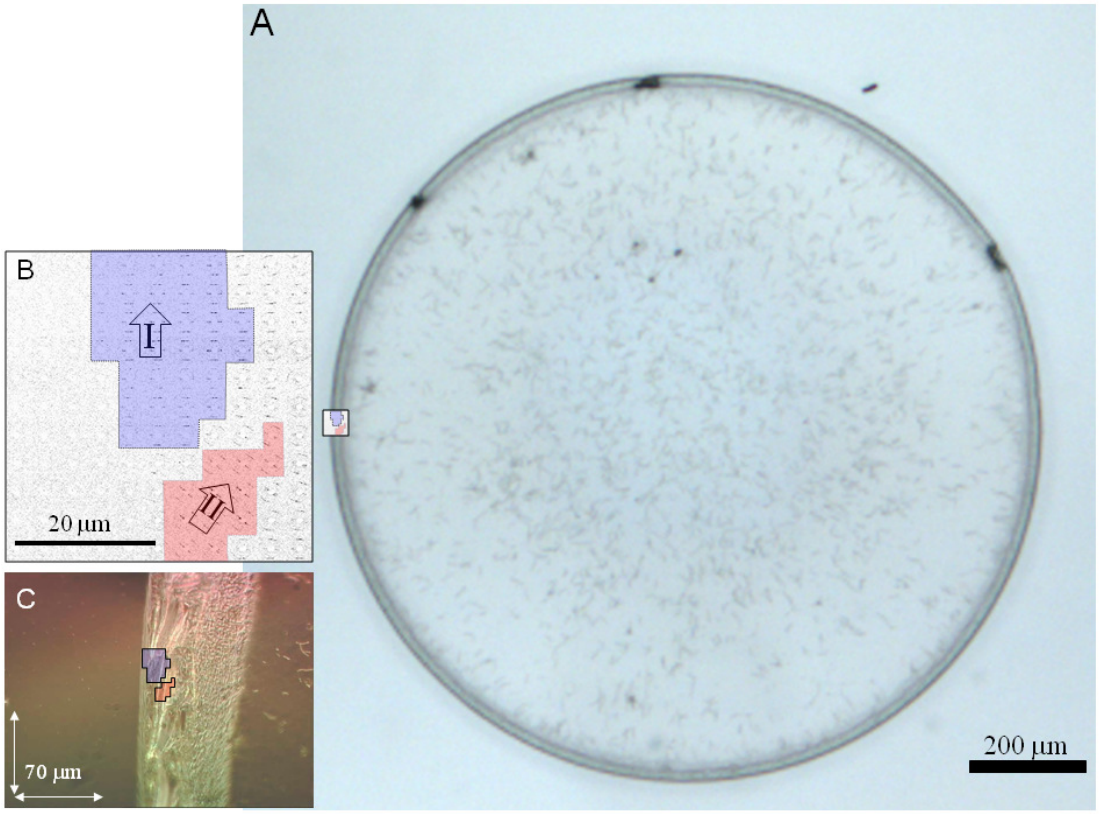

Fig. S3 A: Optical image of cast drop. B: Composite diffraction image based on 4 µm raster-steps revealing two domains (I: blue; II: red) with homogeneous fiber-axis (c-axis) orientation indicated by arrows. C: High resolution optical image (illumination in reflection) of boundary rim revealing homogeneous zones in the outer part. The two domains have been scaled to the optical image © and placed at the outer boundary-rim. The absolute position along the rim-boundary is, however, not known.

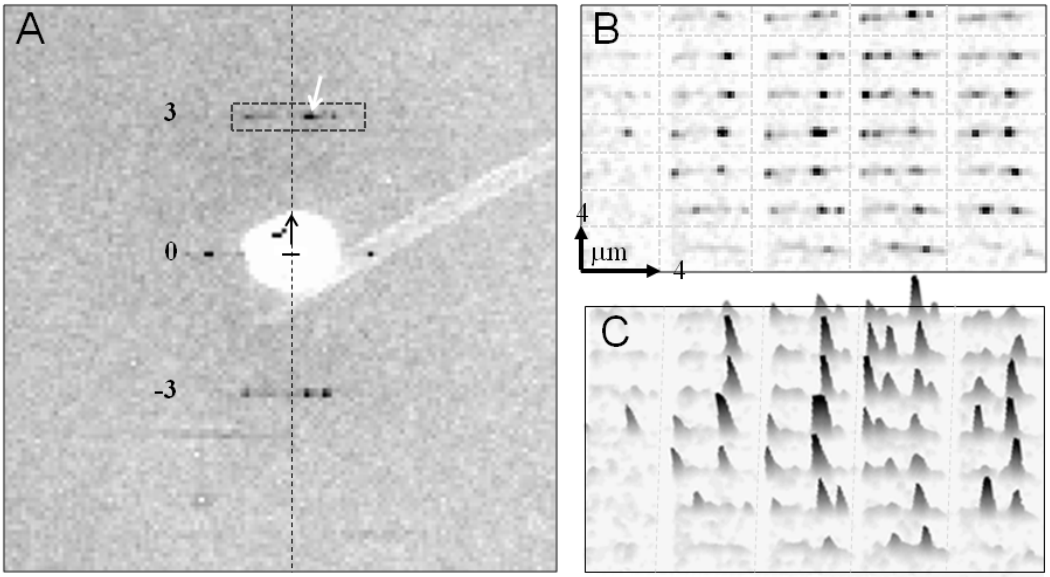

Fig. S4 A: TMV diffraction pattern obtained in transmission-geometry. The "idealized" fiber axis is indicated by a dashed line and an arrow. B: The central part of the n=3 layer line (rectangle) has been selected as pixel for the composite diffraction image based on 4 µm step-increments within domain I (Fig. 2). The white arrow indicates a specific reflection on the n=3 layer-line which was used for generating Fig. S5. C: Pseudo-3D display of composite diffraction image.

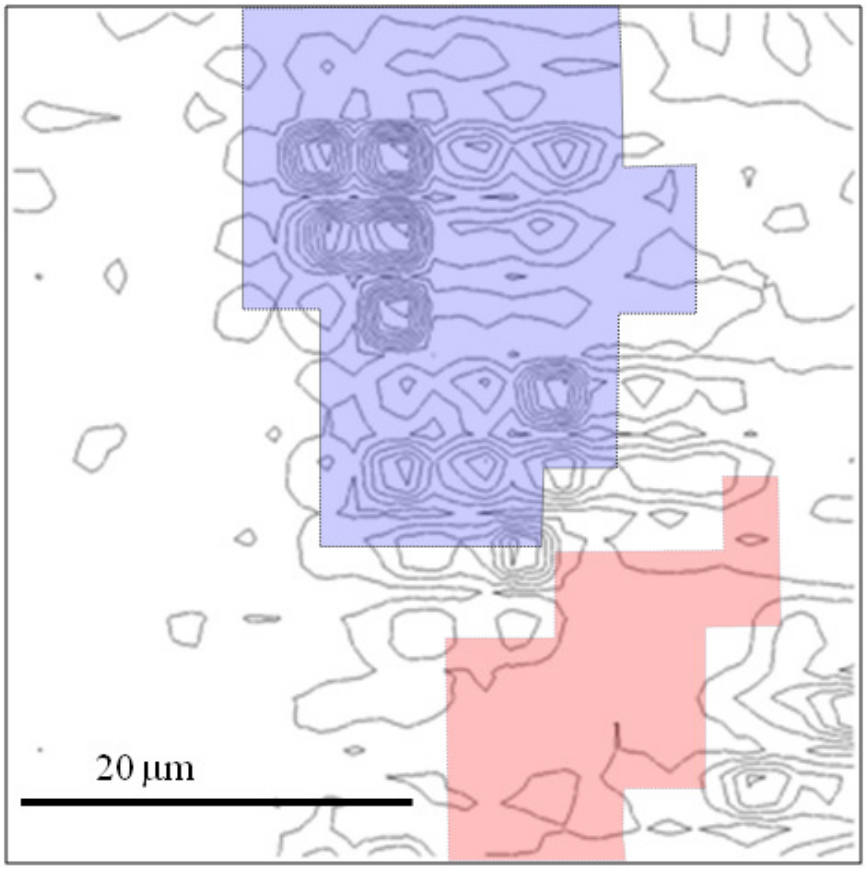

Fig. S5 Composite diffraction image of single n=3 layer line reflection (Fig. S5) displayed as contour map revealing areas of enhanced scattering in domain I (Fig. S3).

We have also calculated a composite diffraction image based on a single n=3 layer-line reflection (white arrow in Fig. S5) in order to spatially locate the enhanced scattering in domain I. Peak intensity integration was performed in a square around the peak-center with ± 1 fwhm of the peak profile range. Enhanced scattering appears to be located at several positions corresponding to the size of single raster-steps. (Fig. 5) We have verified that other reflections on the layer-line correspond to different positions of maximum scattering power in the domain.

Raster reflection-diffraction. A raster-scan in radial direction across the boundary zone with a positional increment of 10 μm is shown in Fig. S6.

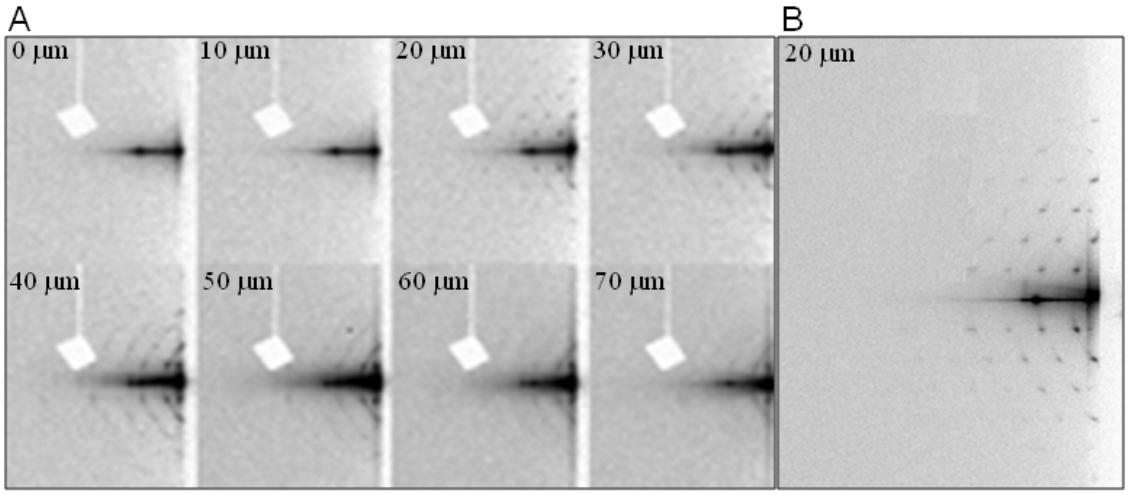

Fig. S6 A: Raster reflection-scan in radial direction with 10 μm increment across the boundary zone of the dried drop. The relative positional increment is indicated. B: Single diffraction pattern from raster-scan.

Well defined peaks can be only seen in one pattern (Fig. S6) while diffuse streaks and split peaks (in other raster-scans) suggest that the beam encounters more or less disordered zones or several smaller domains. This suggests that the large domain studied in reflection geometry is rather an exception while domains with submicron dimensions observed by AFM (Fig. 2) are more common. A higher-resolution raster-scan (not shown) suggests that the radial extension of the highly-ordered domain is less than 1-2 μm, i.e. at the level of the sub-domains observed in transmission-geometry.

Electron-density maps. Low-resolution electron density, difference-density and composite maps based on observed and calculated structure factor amplitudes are shown in Fig. 4D based on TMV fiber diffraction data (PDB ID: 2TMV).[12] Practically identical maps are obtained based on cryo-TEM data for TMV (PDB ID:2OM3).[13] (Fig. S7)

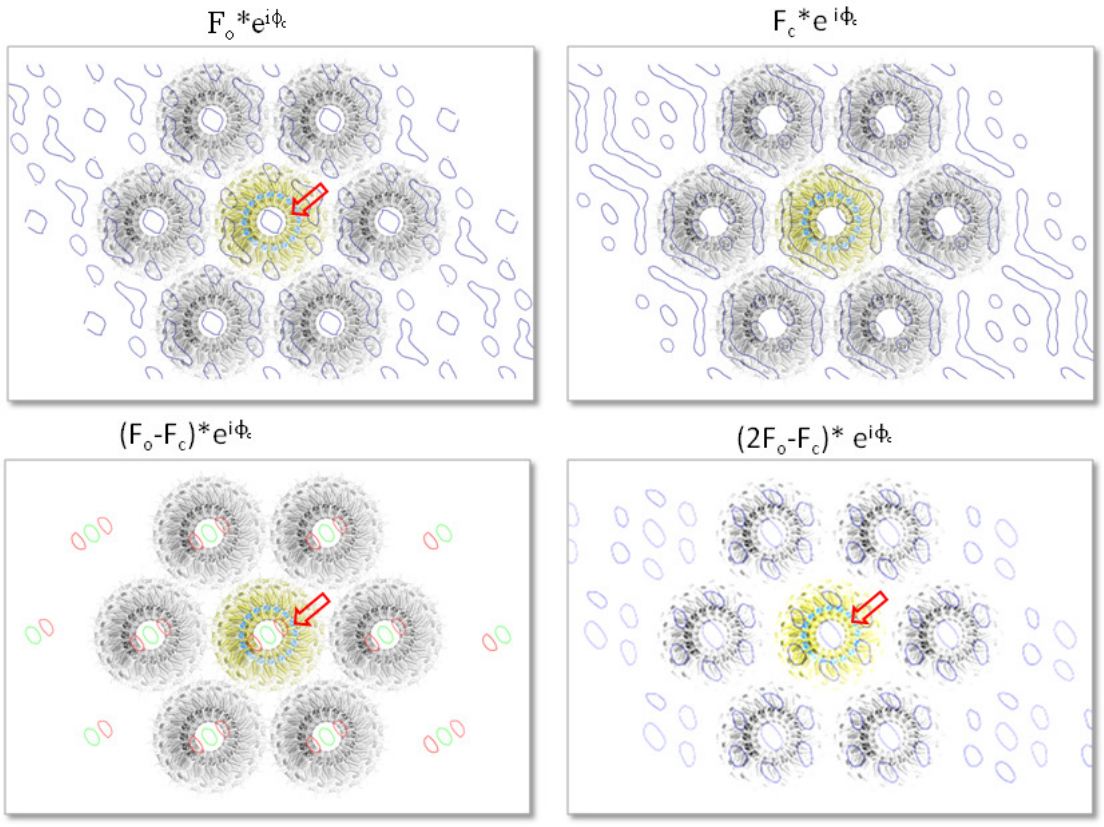

Fig. S7 Electron density, difference- and composite maps based on observed and calculated structure factor amplitudes (F_o, F_c) and phase angles (ϕ_c). (Displayed as P_1 triclinic unit cell) The calculated values were derived from cryo-TEM data (PDB entry: 2OM3).[13] Extra electron density in the central channel visible in the F_{obs} and difference density maps is indicated by a red arrow; blue: electron density contoured at 0.8σ; green : positive difference electron density contoured at +2σ; red : negative difference electron density contoured at - 2σ.

REFERENCES

1. P. Muller-Buschbaum, R. Gebhardt, E. Maurer, E. Bauer, R. Gehrke and W. Doster, *Biomacromolecules*, 2006, **7**, 1773-1780.
2. C. Santos and M. A. R. B. Castanho, *Biophys. J.*, 1996, **71**, 1641-1646.
3. A. Asselin and M. Zaitlin, *Virology*, 1978, **88**, 191-193.
4. D. Necas and P. Klapetek, *Cent Eur J Phys*, 2012, **10**, 181-188.
5. C. Riekel, M. Burghammer, R. Davies, R. Gebhardt and D. Popov, in *Applications of Synchrotron Light to Non-Crystalline Diffraction in Materials and Life Sciences*, eds. M. García-Gutiérrez, A. Nogales, M. Gómez and T. A. Ezquerra, Springer, Heidelberg, 2008.
6. R. Gebhardt, C. Vendrely, M. Burghammer and C. Riekel, *Langmuir*, 2009, **25**, 6307-6311.
7. P. Mueller-Buschbaum, D. Magerl, R. Hengstler, J. F. Moulin, V. Korstgens, A. Diethert, J. Perlich, S. V. Roth, M. Burghammer, C. Riekel, M. Gross, F. Varnik, P. Uhlmann, M. Stamm, J. M. Feldkamp and C. G. Schroer, *J Phys Condens Matter*, 2011, **23**, 184111.
8. T. N. Blanton, T. C. Huang, H. Toraya, C. R. Hubbard, S. B. Robie, D. Louer, H. E. Goebel, G. Will, R. Gilles and T. Raftery, *Power Diffraction*, 1995, **10**, 91-95.
9. J. C. Labiche, O. Mathon, S. Pascarelli, M. A. Newton, G. G. Ferre, C. Curfs, G. Vaughan and A. Homs, *Rev. Scient. Instrum.*, 2007, **78**, 091301-091301 - 091301-

091311.
10. A. Y. Cantillo, *Standard and Reference Materials for Environmental Science*, United States Department of Commerce, Silver Spring, Maryland, USA, 1995.
11. A. Hammersley, *The FIT2D Home Page*, (2009) ESRF, Grenoble.
12. K. Namba, R. Pattanayek and G. Stubbs, *J. Mol. Biol.*, 1989, **208**, 307-325.
13. C. Sachse, J. Z. Chen, P. D. Coureux, M. E. Stroupe, M. Faendrich and N. Grigorieff, *J. Mol. Biol.*, 2007, **371**, 812-835.
14. M. D. Winn, C. C. Ballard, K. D. Cowtan, E. J. Dodson, P. Emsley, P. R. Evans, R. M. Keegan, E. B. Krissinel, A. G. W. Leslie, A. McCoy, S. J. McNicholas, G. N. Murshudov, N. S. Pannu, E. A. Potterton, H. R. Powell, R. J. Read, A. Vagin and K. S. Wilson, *Acta Crystallogr D*, 2011, **67**, 235-242.
15. PyMOL, Schrödinger, LLC, 2013.
16. D. K. G. d. Boer, A. J. G. Leenaers and W. W. v. d. Hoogenhof, *X-Ray Spectrometry*, 1995, **24**, 91-102.